23rd ABCM International Congress of Mechanical Engineering
December 6-11, 2015, Rio de Janeiro, RJ, Brazil

COMPARISON BETWEEN FATIGUE PERFORMANCE OF TWO DIFFERENT AIRCRAFT RIVETED JOINTS

Rynaldo Zanotele Hemerly de Almeida
Instituto de Pesquisas Tecnológicas do Estado de São Paulo – Av. Professor Almeida Prado, 532 São Paulo SP
rynaldo@ipt.br

André Ferrara Carunchio
Roberto Ramos Junior
Escola Politécnica at University of São Paulo – Av. Prof. Mello Moraes, 2231, São Paulo, SP, Brazil – CEP 05508-930
fcarunchio@usp.br, rramosjr@usp.br

Willy Roger de Paula Mendonça
Embraer – Av. Brigadeiro Faria Lima, 1399 São José dos Campos SP
willy.mendonca@embraer.com.br

Abstract. *This work presents results of static and fatigue tests carried out on asymmetric butt riveted joints in order to evaluate their fatigue performances. Two rivet designs largely employed in the aircraft industry were analyzed in aluminum sheet joining: the traditional Briles rivet and the HST11 rivet. In the static tests, specimens were instrumented with strain gages to quantify secondary bending effects induced by the joint asymmetry. The results of these tests partially explain the fatigue performance of the riveted joints. Briles rivet joints presented shorter fatigue life under high loads but longer fatigue life under low loads when compared to HST11 rivet joints. Besides providing fatigue life results for these specific joints, the experiments showed that the fracture location depends on the applied load and may not occur on rivet installation holes despite the stress concentration characteristic of these regions.*

Keywords: *butt-riveted joints, fatigue, aircraft*

1. INTRODUCTION

Although new joining technologies such as FSW (Friction Stir Welding), laser welding and adhesive-bonded joints have achieved promising mechanical properties, riveted joints are still widely employed in aircraft assembly operations due to equipment availability, technology maturity, carrying load capacity and maintenance facility. Furthermore, a broad variety and new rivet designs are available in order to improve both static and fatigue joint performance, and reduce aircraft weight and manufacturing costs.

Due to the diversity of rivet designs, pattern of rivet locations, sheet overlapping configurations and sheet materials, aircraft manufacturers have to carry out specific fatigue tests according to their applications. This work main objective is to compare the fatigue performance of asymmetric butt riveted joints with similar geometries but manufactured with two different rivet designs: the traditional Briles® rivet and the Hi-Lite™ HST11 rivet. Secondly, it provides new inputs for the aircraft joint fatigue database.

Briles rivets, as supplied, consist of one piece conic head and cylindrical body. A second head is formed during assembly operation by squeezing (application of controlled forming force), as depicted in Fig. 1a. In contrast, HST11 rivets, illustrated in Fig. 1b, consist of a piece with a conic head, cylindrical body and threaded body tip, and a second piece, named collar, that is screwed to the threaded body tip in assembly operation. During second head forming, Briles rivet body expands inducing a pretension stress that enhances load transmission and decreases the sensitivity for surface finishing of the hole (Skorupa and Skorupa, 2012; Schijve, 2009; Müller, 1995). Collar screwing to HST11 rivet body compresses sheet against splice increasing the secondary load transfer by friction (Chakherlou *et al.*. 2011). Besides these differences in rivet design, Briles and HST11 rivets are made in Aluminum alloy and Titanium alloy, respectively. Thus, there are expected distinct fatigue performances due to assembly operations and rivet materials.

(a) (b)

Figure 1. Rivet designs: (a) Briles, with formed second head; (b) HST11, with screwed collar (Lisi Aerospace, 2015)

2. MATERIALS AND METHODS

The experiments involved the analysis of large (five rivets per row) and narrow (one rivet per "row") specimens, as illustrated in Fig. 2, manufactured with AA 2524 T3 MRS 1.6 mm thick sheets and 2.0 mm thick splice and the following rivets:

- Briles 14218AD – 5/32'' (AA 2117-T4);
- HST11 5/32'' (Ti6Al4V).

Large specimens were instrumented with strain gages and photoelastic resin, and submitted exclusively to static tests in order to investigate the mechanical behavior of these joints. These results were also used as reference for a finite element modeling validation, presented in a previously published work (Carunchio *et al.*, 2013). Here only selected strain gage results related to the fatigue performance of the analyzed joints are presented.

Fatigue tests were conducted only on narrow specimens. Moreover, narrow specimens were also submitted to static tests to support the definition of fatigue test loads, as explained in the following sections.

Figure 2. Analyzed specimens: (a) large, for instrumented static tests; (b) narrow, for fatigue tests

2.1 Static test procedures and analysis method

When asymmetric riveted joints are loaded, a secondary bending effort is generated due to sheet and splice overlapping (Skorupa and Skorupa, 2012; Schijve, 2009; Müller, 1995). This secondary bending moment increases the tensile stress in the sheets and in the slice on their interface, and reduces the fatigue life of these joints compared to symmetric butt riveted joints (Skorupa and Skorupa, 2012; Schijve, 2009; Müller, 1995).

Static tests were carried out in order to quantify the secondary bending effect. Since its intensity varies along the joint, it is hard to determine it experimentally along all the specimen. However, for two specific regions of interest, it was possible to quantify the ratio between the deformation related to the secondary bending and the deformation related to tensile force, based on strain gages instrumentation.

As shown in Fig. 3, unidirectional strain gages S3 and S14 were installed in opposite faces of the same sheet, aligned with the joint longitudinal direction. Unidirectional strain gages S15, S16 and S17 were installed on the splice, along the joint transverse symmetry plane, aligned with the joint longitudinal direction. Assuming that the combined effect of the tensile force and the secondary bending may be analyzed by the superposition of the separated effects of these efforts, as illustrated in Fig. 4, half of the difference between S3 and S14 measurements corresponds to the bending deformation on this specimen region. The tensile force deformation may be calculated as the mean of S3 and S14 measurements. Thus, one may define the ratio k_{sh} between bending and tensile force deformation portions in this region by Eq. (1).

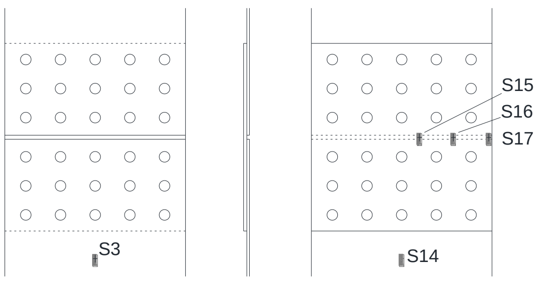

Figure 3. Strain gages of the large specimen instrumentation

However, in the overlapping region, it is not possible to place strain gages on both sides of the splice and, hence, apply the same calculation explained above. But, the cross-section located on strain gages S15, S16 and S17 particularly belongs to the transverse symmetry plane of the specimen and must keep its orientation during the test. Thus, in this cross-section, the force resultant of the stresses in the specimen longitudinal direction must be equal to the external applied tensile load. Assuming again the superposition of bending and traction effects hypothesis, the tensile force 'F'

deformation may be calculated as F/EA, where 'A' and 'E' are the cross-section area and material Young modulus. The bending deformation may be estimated by the difference between the mean of S15, S16 and S17 measurements and the tensile force deformation portion. Therefore, one may define the ratio k_{sp} between bending and tensile force deformation portions in this region by Eqs. (2) and (3).

Six instrumented large specimens, three of each rivet design, were tested using a servo-hydraulic universal testing machine. It was applied a force mode control and the load profile consisted in load ramps equivalent to 4 MPa/s intercalated with constant load dwells. This load profile was useful considering other aspects not included in this work (particularly the photoelastic instrumentation). Concerning the presented analysis, one may focus on the load monotonic increasing characteristic.

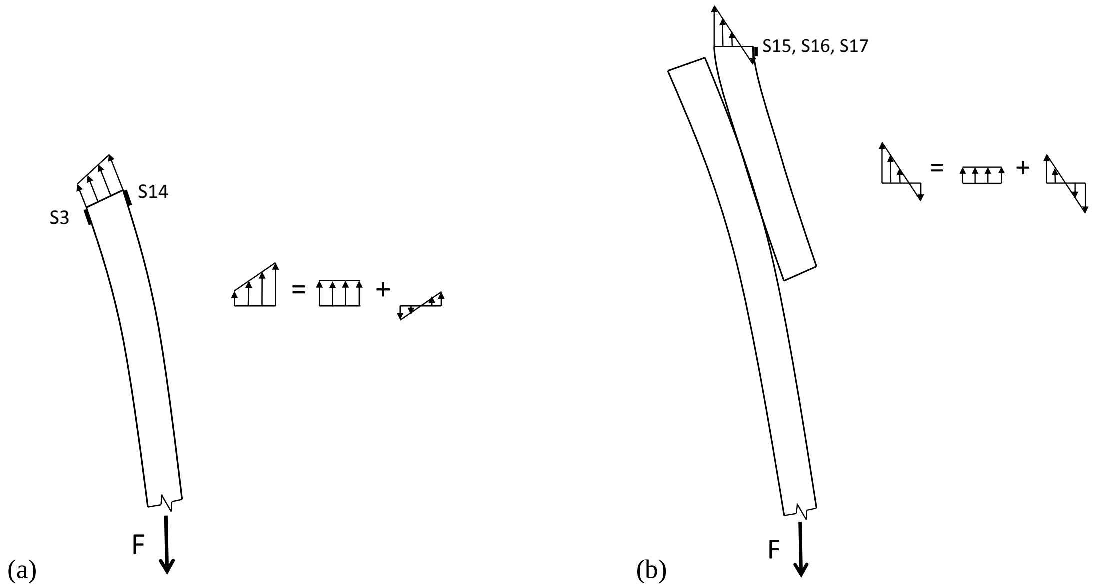

Figure 4. Stress profiles: (a) sheet cross-section on S3 and S14 strain gages; (b) splice cross-section on S15, S16 and S17

$$k_{sh} = \frac{(S14 - S3)/2}{(S14 + S3)/2} \quad (1)$$

$$k_{sp} = \frac{|\bar{S} - F/EA|}{F/EA} \quad (2)$$

$$\bar{S} = \frac{S15 + S16 + S17}{3} \quad (3)$$

2.2 Fatigue test procedures and analysis method

For each rivet design, 25 narrow specimens were tested in order to determine fatigue life curves in the range 10,000 to 2,000,000 cycles. Based on MIL-STD-1312-21 (1985), nominal stress levels of 220 MPa, 160 MPa, 90 MPa were initially defined. These loads correspond to approximately 70%, 50% and 30% of the joint ultimate load. The joint ultimate load was estimated as the mean of ultimate loads obtained in static tests of four narrow specimens (two of each rivet design). Five narrow specimens of each rivet design were tested under those three nominal stress levels. The remaining nominal stress levels were estimated in order to reach the desired life range.

Here, the nominal stress level corresponds to the maximum load during cycle over the sheet gross cross-section area. The minimum cycle load was determined as 10% of the maximum cycle load ('r' ratio equals to 0.1), keeping the specimen under traction during the entire cycle.

After the specimen fracture or a 2,500,000 cycle limit achievement (run-out criteria), a SN curve for each rivet design was obtained by data fitting based on the expression proposed in Eq. (4), where S stands for nominal stress level, N for fatigue life cycles, r for the minimum over maximum cycle load ratio and A_i for coefficients to be determined.

$$\log(N) = A_1 + A_2 \log(S(1-r)^{A_3} - A_4) \quad (4)$$

3. RESULTS

In this section, large specimens using Briles and HST11 rivets were identified as IA-X and IB-X, respectively, where 'X' varies from 1 to 3. Narrow specimens were identified as IA-YY (Briles specimens) and IB-YY (HST11 specimens), where 'YY' may vary from 02 to 28.

3.1 Static test results

The ratios k_{sh} and k_{sp} were calculated for each specimen based on strain gages measurements. These results as well as their mean, according to specimen rivet design are shown in Figs. 5 and 6 for applied nominal stress in the range 5 MPa to 250 MPa. Particularly for Briles rivets, the mean was calculated from the results of specimens IA-1 and IA-3 only, due to the larger discrepancy between IA-2 specimen results and the other results.

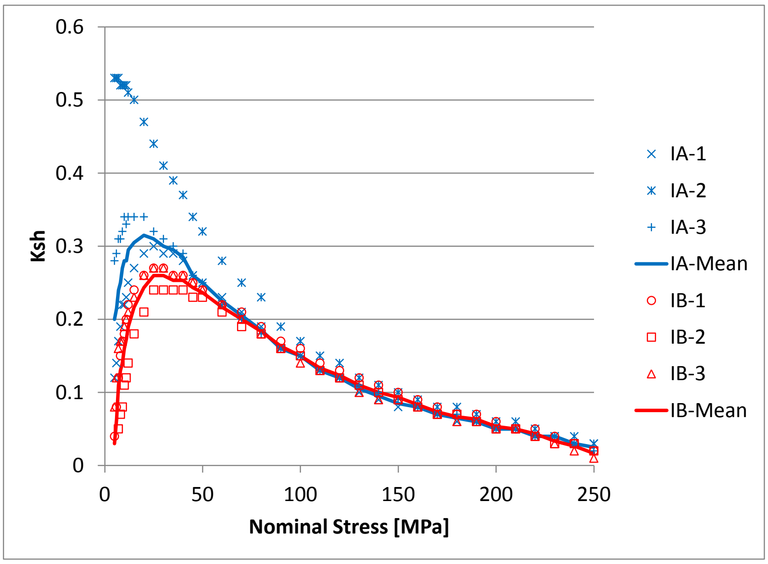

Figure 5. Ratio k_{sh} between bending and tensile force effects in sheet near S3 and S14 strain gages

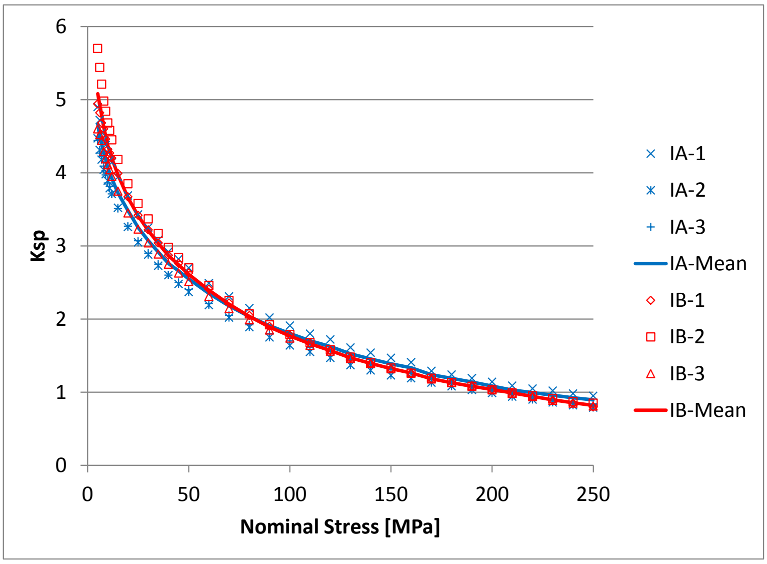

Figure 6. Ratio k_{sp} between bending and tensile force effects in splice near S15, S16 and S17 strain gages

In both figures it can be observed that the bending effect decreases when the nominal stress increases. This is a consequence of the specimen deflection that tends to diminish the bending moment arm. For low nominal stresses, there is a peak in k_{sh} in the order of 0.3 around 30 MPa and an exponential increasing of k_{sp} when the nominal stress goes to zero. This is in accordance with similar results presented by Müller (1995). Near 80 MPa, k_{sp} equals to 2. This means that the maximum deformation in the transverse symmetry plane of the splice is 3 times the tensile force deformation in this cross-section. Just for comparison purposes, it can be noticed that this relation has the same magnitude of the stress concentration factor around a circular hole in a sheet under tension (classical Kirsch problem).

The difference between k_{sh} for each rivet design is visible for low nominal stresses. However, for nominal stresses above 80 MPa, it is hard to distinguish the two k_{sh} curves. Concerning k_{sp} results, no relevant differences can be found in Fig. 6. But, in a more careful analysis, one can observe that the HST11 rivet curve is slightly above the Briles rivet curve for nominal stresses up to 80 MPa and slightly below the Briles rivet curve for higher nominal stresses. To clarify this argument, the ratio between the mean k_{sp} of HST11 specimens and the mean k_{sp} of Briles specimens was calculated and presented in Fig. 7.

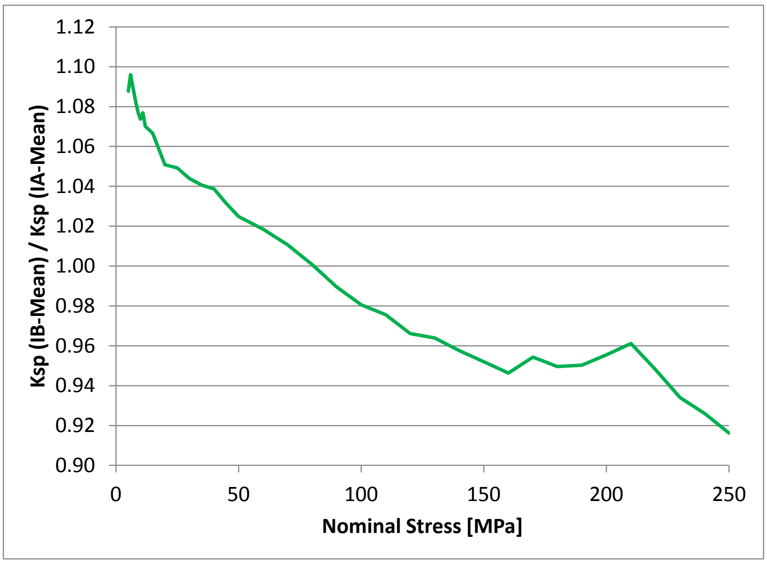

Figure 7. Ratio between the mean k_{sp} of HST11 specimens and the mean k_{sp} of Briles specimens

One can observe that k_{sp} for the mean of HST11 results consistently varies from approximately plus 10% to minus 10% of k_{sp} for the mean of Briles results.

3.2 Fatigue test results

The fitted SN curves according to Eq. (4) are shown in Fig. 8. Life cycles and fracture locations are listed in Tab. 1 and 2 for Briles and HST11 rivets, respectively. Figures 9 to 14 show selected fractured specimens and their corresponding fractured cross-sections. The following codification was employed to identify fracture locations:

- SH-OP: **SH**heet, **O**n a **P**eripheral rivet row;
- SP-OC: **SP**lice, **O**n a **C**entral rivet row.
- SP-NC: **SP**lice, **N**ear a **C**entral rivet row;
- SP-BC: **SP**lice, **B**etween **C**entral rivet rows;
- Run-out: 2,500,000 cycles limit reached.

Figure 8 shows that under high loads (220 MPa nominal stress), fatigue lives of HST11 specimens are longer than those of Briles specimens. However, below a nominal stress of 150 MPa, Briles specimens become more fatigue resistant than HST11 specimens. This characteristic cannot be completely explained by static tests results, but poorer HST11 results under low loads may be related to greater values of HST11 specimen k_{sp}, as shown in Fig. 6 and 7, that indicated a higher secondary bending effect on these rivet design specimens under low loads. Probably, the difference between rivet flexibilities, associated with joint geometries, leads to nonlinear relations between applied load and load distributions among rivet rows that culminates with the SN curves crossing. But, further investigation is necessary to support this hypothesis. In accordance with static test analyses, the fracture location tends to occur on a joint sheet under high loads and on splice under low loads. Fractures in sheets always occurred on a peripheral rivet row; but, in splice, fractures occurred on central rivet row and full cross section positions. Specifically for Briles rivets, some specimen splices fractured between two central rivet rows, as shown in Fig. 11a, relatively far from stress concentration regions of rivet installation holes. This confirms that the secondary bending effect may be more significant than stress concentration around holes and indicates that the region near the joint transverse symmetry plane is the most affected by secondary bending in Briles specimens under low load.

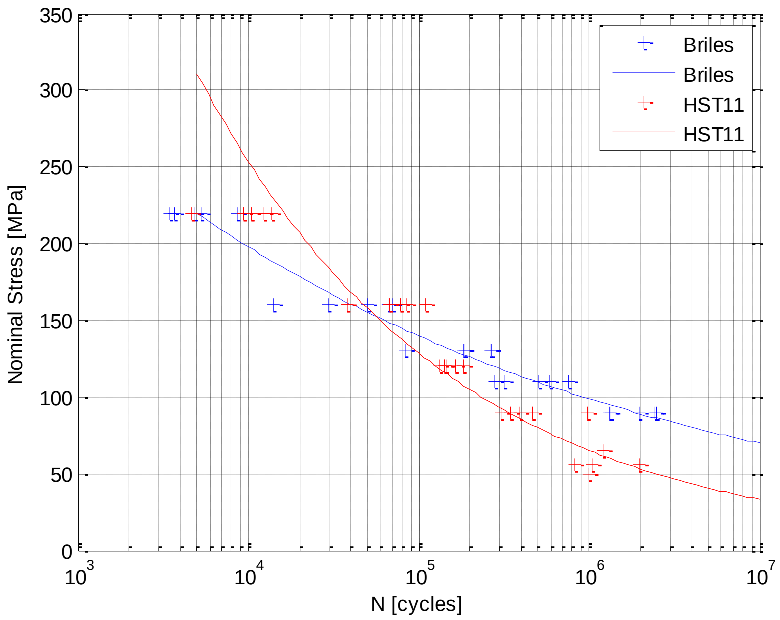

Figure 8. SN curves for Briles and HST11 specimens

Table 1. Briles rivets fatigue test results.

Nominal Stress [MPa]	Specimen ID	N [cycles]	Failure location
220	IA-03	3436	SH-OP
	IA-06	3678	
	IA-04	4877	
	IA-12	5314	
	IA-13	8569	
160	IA-15	13970	SH-OP
	IA-09	29260	
	IA-07	49772	
	IA-14	66331	
	IA-08	70966	
130	IA-18	83611	SH-OP
	IA-22	183542	
	IA-19	188353	
	IA-20	263411	SP-NC
	IA-21	267264	
110	IA-23	589769	SP-BC
	IA-27	754670	
	IA-26	321150	SP-OC
	IA-25	504290	
	IA-24	278990	SH-OP
90	IA-11	1322316	SP-BC
	IA-10	1335328	
	IA-17	2440445	
	IA-02	1989816	SP-OC
	IA-16	2500000	*Runout*

Table 2. HST11 rivets fatigue test results.

Nominal Stress [MPa]	Specimen ID	N [cycles]	Failure location
220	IB-05	4674	SH-OP
	IB-04	9379	
	IB-13	10343	
	IB-09	12426	
	IB-14	13655	
160	IB-06	37734	SH-OP
	IB-15	67747	
	IB-08	77920	
	IB-16	85994	
	IB-07	109178	SP-NC
120	IB-23	141672	SP-NC
	IB-19	145193	
	IB-20	164730	
	IB-22	132307	SH-OP
	IB-21	181439	
90	IB-11	307575	SP-NC
	IB-17	343668	
	IB-12	392994	
	IB-10	461873	
	IB-18	973999	
65	IB-24	1208795	SP-NC
56	IB-27	825064	
	IB-26	1032816	
	IB-25	1957058	
50	IB-28	1006170	

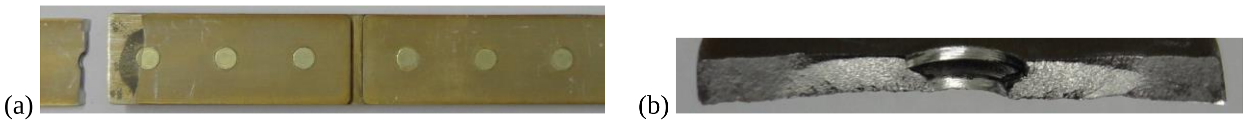

Figure 9. Specimen IA-19 (130 MPa): (a) fracture SH-OP; (b) fractured cross-section

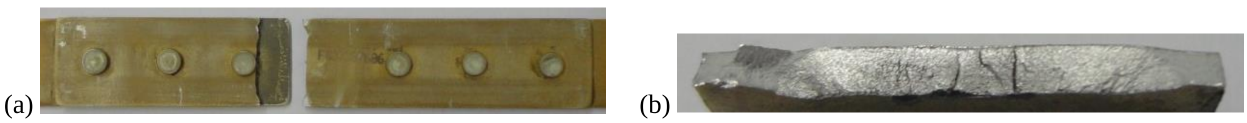

Figure 10. Specimen IA-21 (130 MPa): (a) fracture SP-NC; (b) fractured cross-section

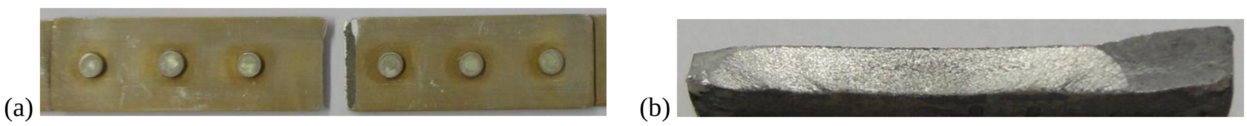

Figure 11. Specimen IA-10 (90 MPa): (a) fracture SP-BC; (b) fractured cross-section

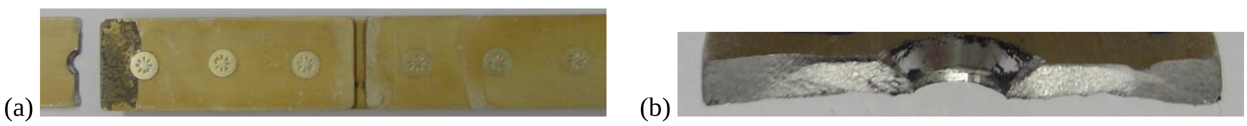

Figure 12. Specimen IB-22 (120 MPa): (a) fracture SH-OP; (b) fractured cross-section

(a) (b)
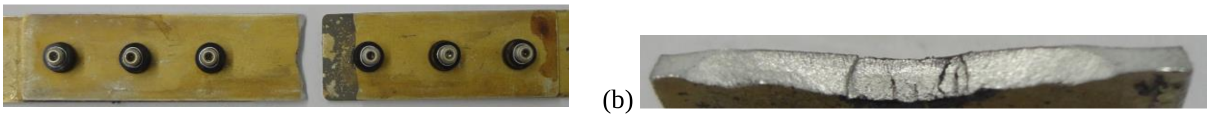

Figure 13. Specimen IB-19 (120 MPa): (a) fracture SP-NC; (b) fractured cross-section

(a) (b)
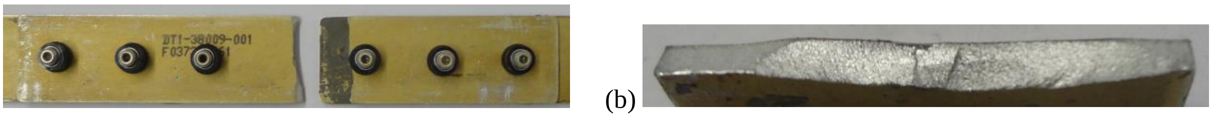

Figure 14. Specimen IB-17 (90 MPa): (a) fracture SP-NC; (b) fractured cross-section

In all fractured cross-sections pictures presented in Fig. 9b to 14b, the interface between sheet and splice is on the bottom cross-section edge. Thus, analyzing the beach marks, it can be concluded that the crack nucleation always occurred in that region. This is a consequence of the secondary bending that increases tension stresses for both sheet and splice on their interface. Also, the crack nucleation usually started on or near a rivet installation hole due to the stress concentration in these regions. Indeed, in most splice fractures, one can observe marks of neighbor crack linking, characteristic of stress concentration regions, where multiple crack nucleation may occur. However, for Briles rivet specimens under low load (90 MPa), the fracture was located in the splice between central rivet rows, relatively far from stress concentration areas. Therefore, a smoother fracture cross-section was obtained, as shown in Fig. 11b. This is probably related to higher fatigue lives of Briles rivet specimens under low loads when compared to HST11 rivet specimens lives.

4. CONCLUSIONS

The fatigue tests pointed out that the fracture location depends on the applied load for specimens of both rivet designs. Usually, the fracture occurs on a joint sheet under high loads and on splice under low loads. Indeed, it could be observed in static test results that the secondary bending greatly affects splice under low loads.

Briles rivet joints presented shorter fatigue life under high loads but longer fatigue life under low loads when compared to HST11 rivet joints, possibly due to different rivet flexibilities. Although some difference was observed on static tests results of specimens of the two rivet designs, they were not sufficient to completely explain the two SN curves crossing. Probably, the induced residual stresses affect more intensively a narrower region around the holes then that monitored with strain gages.

The fracture beach marks indicated that the crack nucleation always occurred in the interface between sheet and splice, and, in most cases, near or on a rivet hole. This was expected due to secondary bending and stress concentration around hole. However, the secondary bending effect in the splice transverse symmetry plane may be more significant than stress concentration around holes and may unexpectedly shift the fracture location to that full cross section region.

5. REFERENCES

Carunchio, A. F., Driemeier, L., Ramos Jr, R., Almeida, R. Z. H., Mendonça, W. R. P., 2013. "Numerical and experimental analysis of riveted joints for aeronautical applications". In *Proceedings of the 22st International Congress of Mechanical Engineering -COBEM2013*. Ribeirão Preto, Brazil.

Chakherlou, T. N., Razavi, M. J., Aghdam, A. B., 2011. "On the variation of clamping force in bolted double lap joints subjected to longitudinal loading: a numerical and experimental investigation". *Strain*, Vol. 48, pp. 21-29.

Lisi Aerospace, 2015. "Hi-Lite^{TM} Pin". 5 May, 2015 <http://www.lisi-aerospace.com/products/fasteners/externally-threaded/pin/Pages/hi-lite.aspx>

MIL-STD-1312-21, 1985. *Fastener test methods, Method 21, Shear joint fatigue – Constant amplitude*. Military Standard, Department of Defense – USA, Washington.

Müller, R. P. G., 1995. *An experimental and analytical investigation on the fatigue behaviour of fuselage riveted lap joints*. Ph.D. thesis, Faculty of Aerospace Enginnering of Delft University of Technology, Delft.

Schijve, J., 2009. *Fatigue of Structures and Materials*. Springer, Berlin, 2nd edition.

Skorupa, A., Skorupa, M., 2012. *Riveted Lap Joints in Aircraft Fuselage*. Springer, Berlin, 1st edition.

6. RESPONSIBILITY NOTICE

The authors are the only responsible for the printed material included in this paper.